Supporting Information

Integrating oxophilic and protophilic properties on multivalent $Co_9S_8@CoMoP_x$ electrode to boost alkaline hydrogen evolution

Xijie Chen,[a] Fengming Zhang,[a] Xiao Wang,[a] Fangming Liu,[a] Jinhan Li,[a] Meng Yu,[*a] Fangyi Cheng[*ab]

[a] *Key Laboratory of Advanced Energy Materials Chemistry (Ministry of Education), Engineering Research Center of High-efficiency Energy Storage (Ministry of Education), College of Chemistry, Nankai University, Tianjin 300071, China;*

[b] *Haihe Laboratory of Sustainable Chemical Transformations, Tianjin 300192, China.*

[*] Corresponding authors.
E-mail address: nkyu2023@nankai.edu.cn (M. Yu), fycheng@nankai.edu.cn (F. Cheng).

1 Experimental

1.1 Materials and Measurements

CoSO$_4$·7H$_2$O (99% metals basis), Na$_2$MoO$_4$·2H$_2$O (99% metals basis), NaH$_2$PO$_2$·H$_2$O (99%), C$_6$H$_5$O$_7$Na$_3$ (98%) and Na$_2$S$_2$O$_3$·5H$_2$O (99.5%) were purchased from Aladdin. The conductive substrate used in this work is nickel foam (NF, Sinero) with the thickness of 0.5 mm. All the above reagents were used as received unless otherwise noted.

Scanning electron microscopy (SEM) equipped with an energy-dispersive X-ray spectroscopy (EDS) was performed in JEOL JSM-7900F microscope. Transmission electron microscopy (TEM) with EDS and selected area electron diffraction (SAED) system was conducted on FEI Talos F200X G2 microscope. X-ray diffraction (XRD) measurements were conducted using a Rigaku Mini Flex 600 powdered with Cu-Kα radiation. X-ray photoelectron spectroscopy (XPS) were carried out on AXIS ULTRA employing Al-Kα X-ray source. Raman measurements were performed with a confocal Raman microscope (LabRAM HR Evolution, Horiba) with 532 nm laser. The atomic ratio of materials and metal ions concentration in the electrolyte were detected by the inductively coupled plasma-optical emission spectrometry (ICP-OES, SpectroBlue).

1.2 Synthesis of self-supported electrocatalysts

1.2.1 Synthesis of Co$_9$S$_8$@CoMoP$_x$ electrode

Co$_9$S$_8$@CoMoP$_x$ was prepared on NF by continuous two-step electrodeposition method. Before electrodeposition, NF was treated by ethanol, 3 M HCl and deionized water in sequence. The pretreated NF and graphite rod were used as working and counter electrode, respectively. The deposition electrolyte for the bottom CoMoP$_x$ is: 45 mM CoSO$_4$·7H$_2$O, 15 mM Na$_2$MoO$_4$·2H$_2$O, 0.5 M NaH$_2$PO$_2$·H$_2$O and 0.15 M Na$_3$C$_6$H$_5$O$_7$, in which CoSO$_4$·7H$_2$O and Na$_2$MoO$_4$·2H$_2$O provide Co and Mo source, and NaH$_2$PO$_2$·H$_2$O is regarded as both P source and reductant. The Na$_3$C$_6$H$_5$O$_7$ serves as the complexing agent for the active deposition of metal ions. The first electrodeposition was carried out at constant current density of −0.1 A cm^{-2} for 5~20 min, and argon gas was continuously injected into the deposition solution. The prepared electrode was cleaned with deionized water and dried at 60 °C in a vacuum oven to obtain the self-supported CoMoP$_x$ electrode. Then, the CoMoP$_x$ was immersed in the second deposition electrolyte containing 0.05M CoSO$_4$·7H$_2$O, 0.1 M Na$_2$MoO$_4$·2H$_2$O and deposited at −10 mA cm^{-2} for 1~4 min. After cleaning and drying, the Co$_9$S$_8$@CMP cathode with different layer thickness was obtained.

1.2.2 Synthesis of other electrocatalysts

CoMoP$_x$, Co$_9$S$_8$ and CoP self-supported electrodes were prepared by one-step electrodeposition. The deposition electrolyte of the CoMoP$_x$ electrode is described in section 1.2.1, and was obtained by cathode current deposition with -0.1 A cm^{-2} for 15 min. The deposition electrolyte of Co$_9$S$_8$ catalyst is also same as that in section 1.2.1, with deposition condition of -10 mA cm^{-2} for 3 min. CoP was prepared at -10 mA cm^{-2} for 10 min in the electrolyte containing 25 mM CoSO$_4$·7H$_2$O, 0.5 M NaH$_2$PO$_2$·H$_2$O and 0.1 M Na$_2$MoO$_4$·2H$_2$O without Mo source.

### 1.3 Electrochemical measurements

The electrochemical measurements were carried out on Ivium-n-Stat using standard three-electrode system with as-prepared self-supported electrocatalysts, Hg/HgO electrode and Pt foil as working, reference and counter electrode, respectively. The polarization curves were collected in 1.0 M KOH solution with scan rate of 10 mV s^{-1} for linear sweep voltammetry (LSV) and 50 mV s^{-1} for cyclic voltammetry (CV) curves. Electrochemical impedance spectroscopy (EIS) measurement was performed with frequencies ranging from 100 kHz to 0.1 Hz and an amplitude of 10 mV. Operando EIS measurement was carried out by applying the overpotential from 0 to 180 mV with an interval of 20 mV vs. RHE in 1.0 M KOH. The catalytic stability of the electrode was operated by chronoamperometry and accelerated degradation tests. All the above measured potentials were converted to the reversible hydrogen electrode (vs. RHE) according to the equation:

$$E_{VS.RHE} = E_{VS.SCE} + E_{SCE}^{\theta} + 0.059 \times pH$$

1.3 Assembly of anion exchange membrane water electrolysis device

The commercial Alkymer W-25 anion exchange membrane (AEM) with the thickness of 50 μm was employed. It is worth noting that the size of the AEM should be slightly larger than serpentine channel inside the end plate to avoid short circuit and electrolyte leakage. Thus, the AEM was cropped to 3.5×3.5 cm^2 and immersed into 1.0 M KOH for 12~24 h to achieve efficacious OH$^-$ conductivity. The activated AEM was then rinsed with deionized water for further use. The Co$_9$S$_8$@CoMoP$_x$ and Ni$_3$S$_2$@NFP electrode with the size of 2×2 cm^2 was used as cathode and anode, respectively. The monolithic membrane electrode assembly (MEA) involved three sections with the sandwich structure that AEM membrane in the middle and electrodes on both sides, which was then hot pressing with 1 MPa for 1 min at 40 °C.
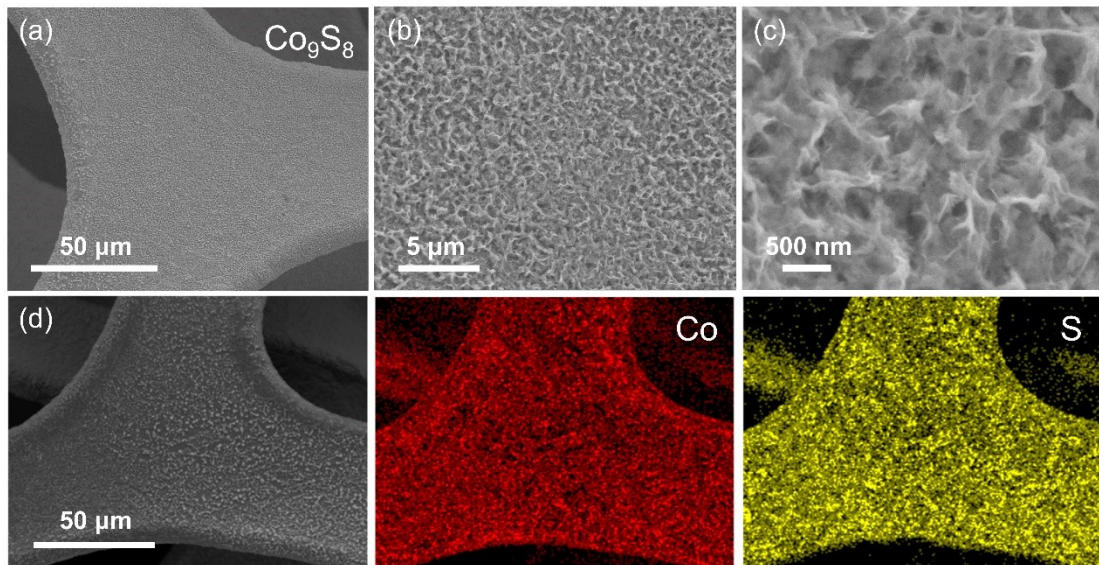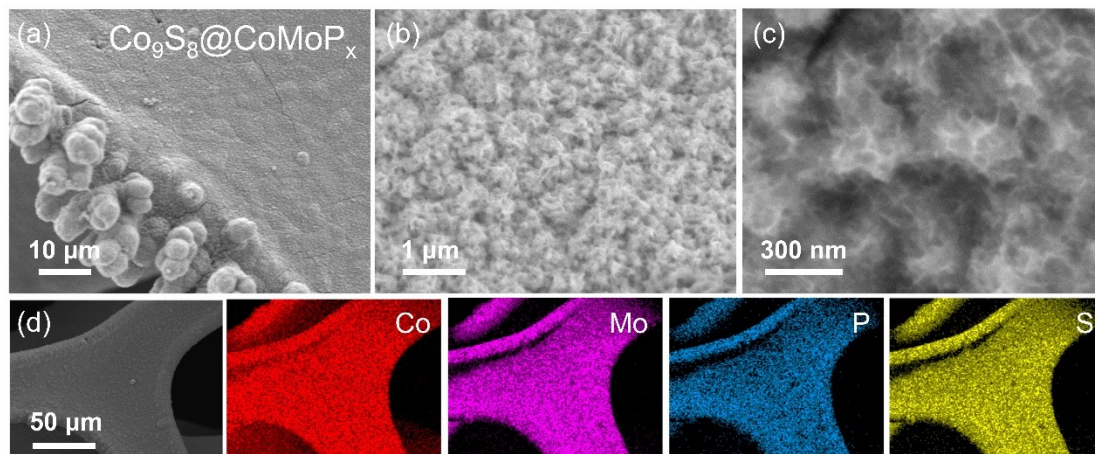
2 Results and Discussion
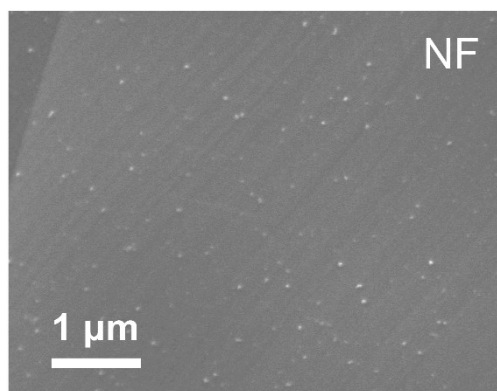
Fig. S1. SEM images of blank NF.
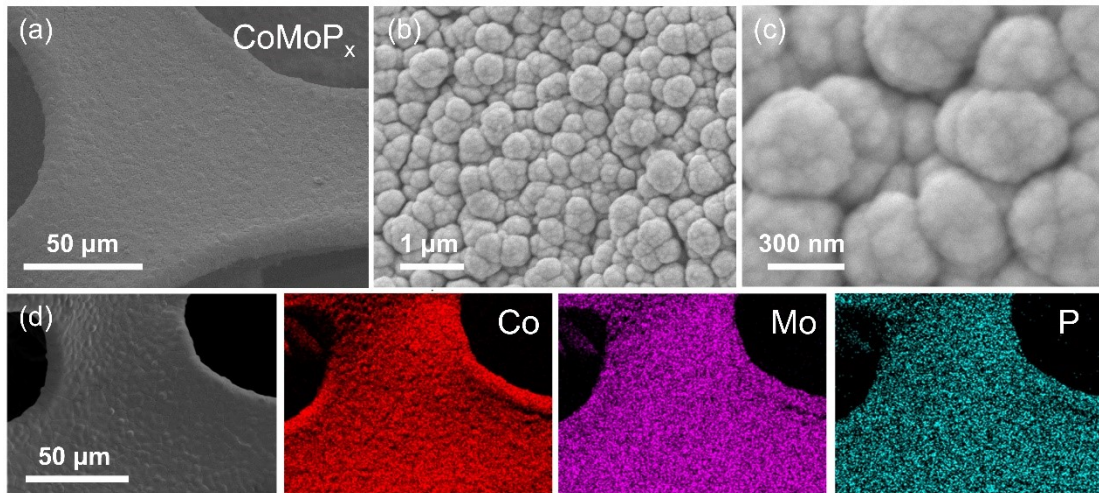
Fig. S2. (a-c) The SEM images of $CoMoP_x$ under different magnifications and (d) the corresponding EDS elemental mappings of Co, Mo and P elements.
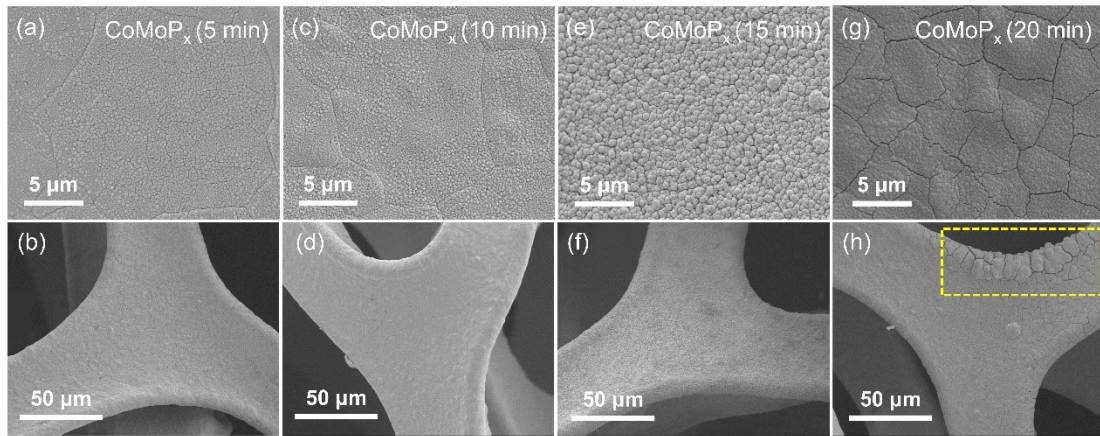
Fig. S3. (a-c) The SEM images of Co_9S_8 under different magnifications and (d) the corresponding EDS mappings of Co and S elements.
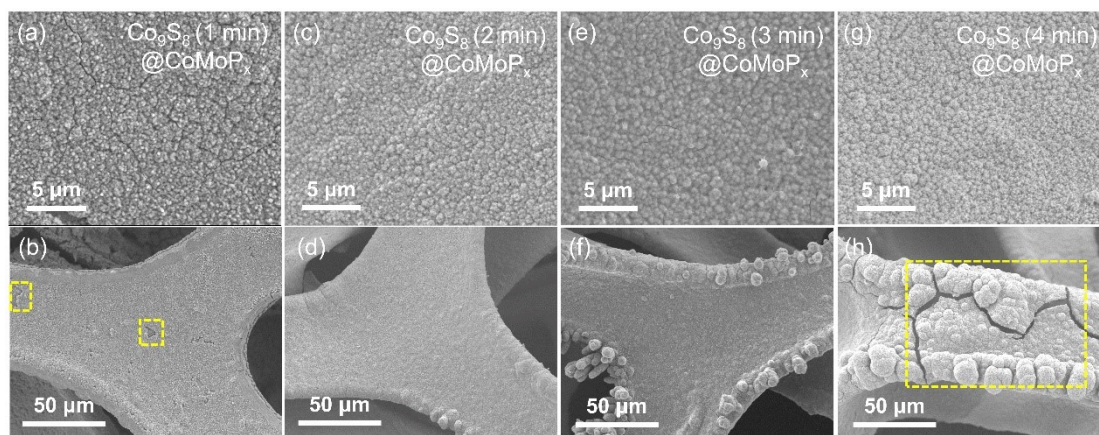
Fig. S4. (a-c) The SEM images of $Co_9S_8@CoMoP_x$ under different magnifications and (d) the corresponding EDS mappings of Co, Mo, P and S elements.

As shown in Fig. S4, simultaneously exposure of Mo, P and S elements in EDS mappings for $Co_9S_8@CoMoP_x$, which can be attribute to that surface Co_9S_8 with almost nanosheet clusters morphology cannot completely restrain detection of high-energy electron beam. In addition, given that the sampling depth of EDS is about 1 μm or so, it is possible to observe Mo signals in the elemental mapping, even in the regions covered by Co_9S_8, creating the coexistence of components.

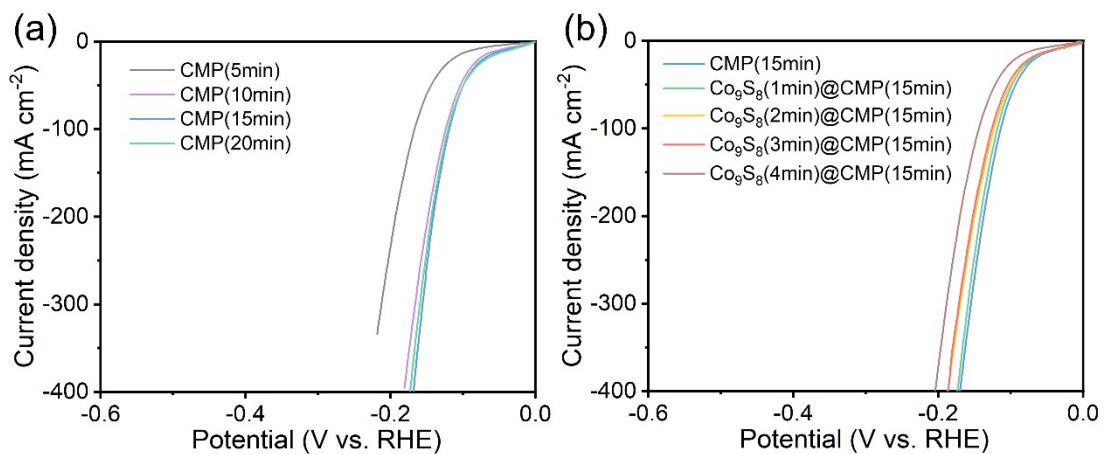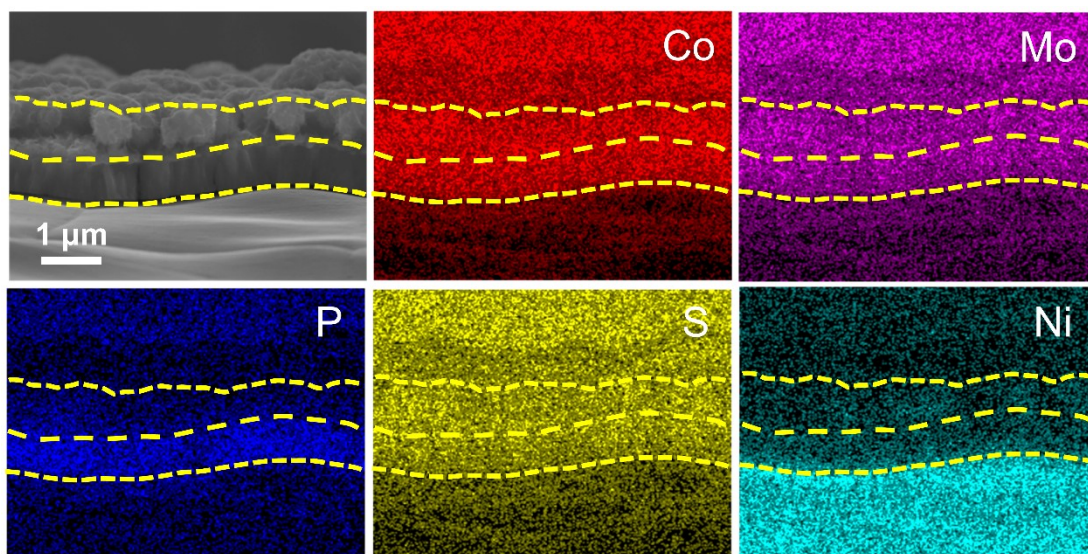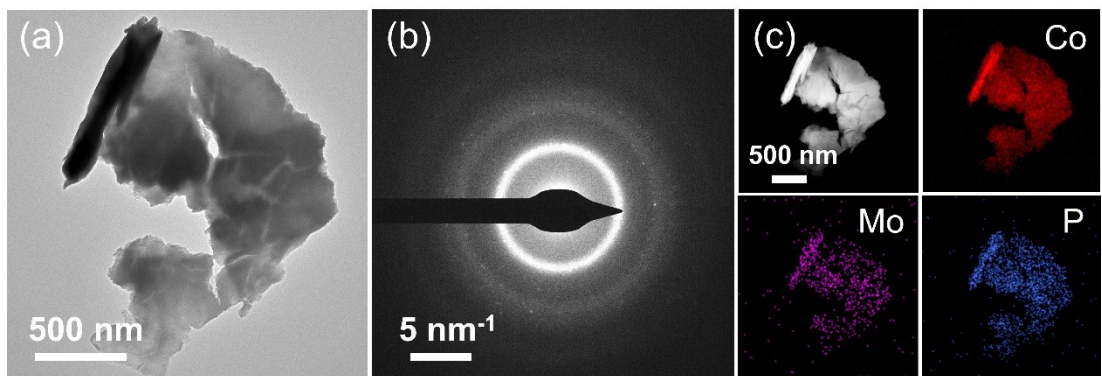**Fig. S5.** The SEM images of CoMoP$_x$ with different deposition times.

Fig. S6. The SEM images of $Co_9S_8@CoMoP_x$ with different deposition times of surface Co_9S_8.
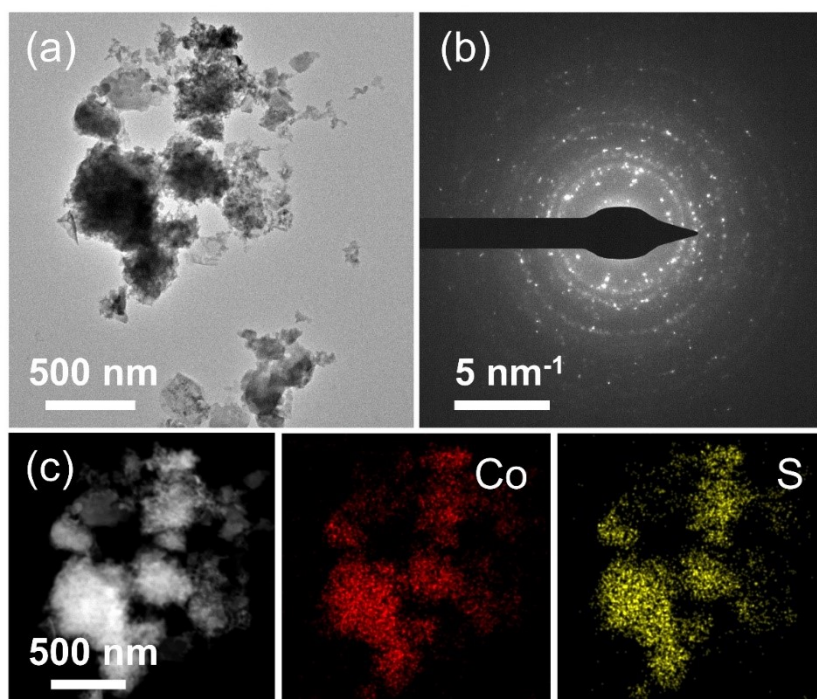
**Fig. S7.** The LSV curves of $Co_9S_8@CoMoP_x$ with different deposition times of (a) $CoMoP_x$ and (b) Co_9S_8.

**Fig. S8.** The cross-section EDS mappings of $Co_9S_8@CoMoP_x$.

Fig. S9. (a) The TEM images and (b) selected area electron diffraction (SAED) pattern of CoMoP$_x$. (c) The corresponding EDS elemental mappings of Co, Mo and P elements.

Fig. S10. (a) The TEM images and (b) selected area electron diffraction (SAED) pattern of Co_9S_8. (c) The corresponding EDS elemental mappings of Co and S elements.
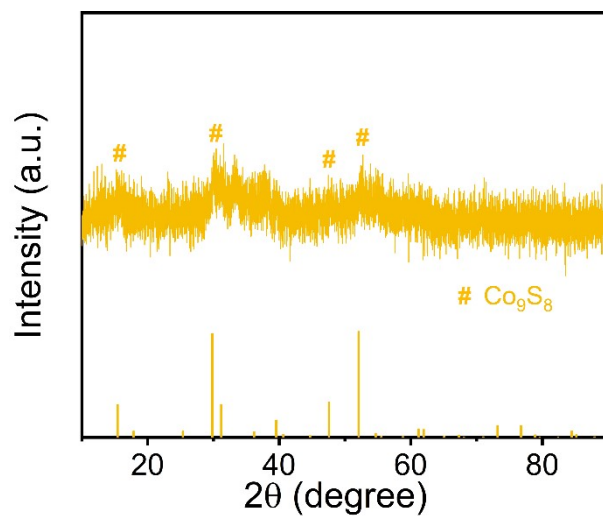
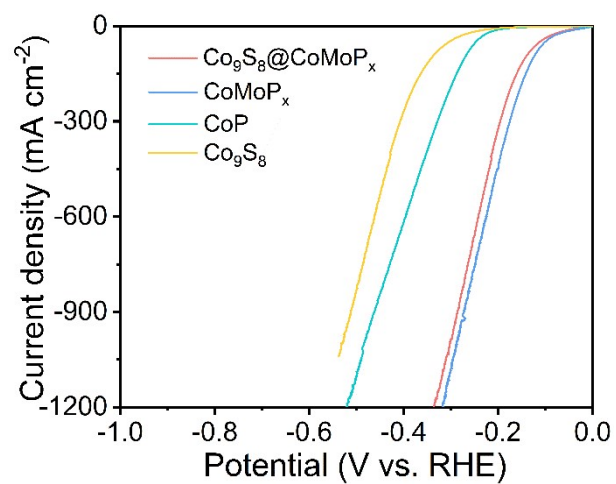**Fig. S11.** The XRD pattern of Co_9S_8.
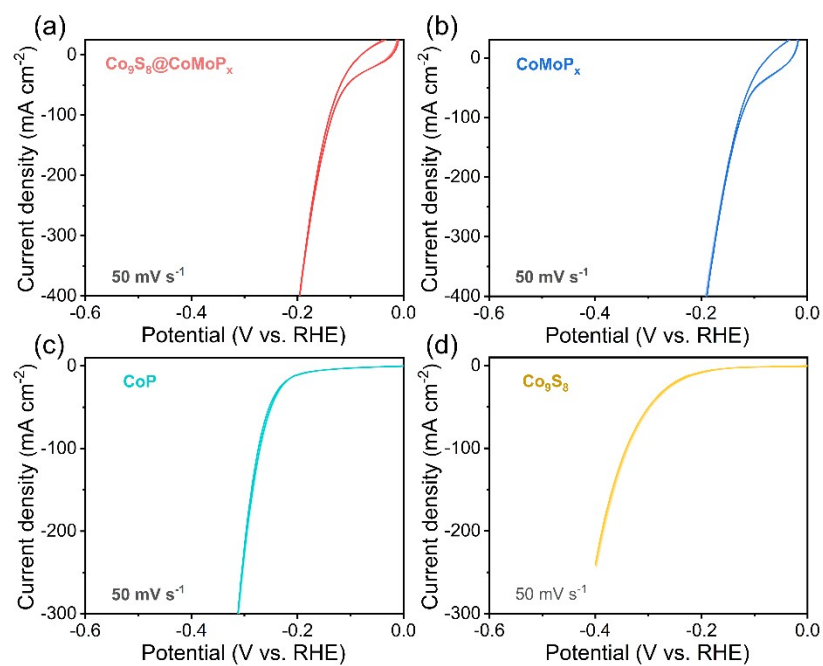
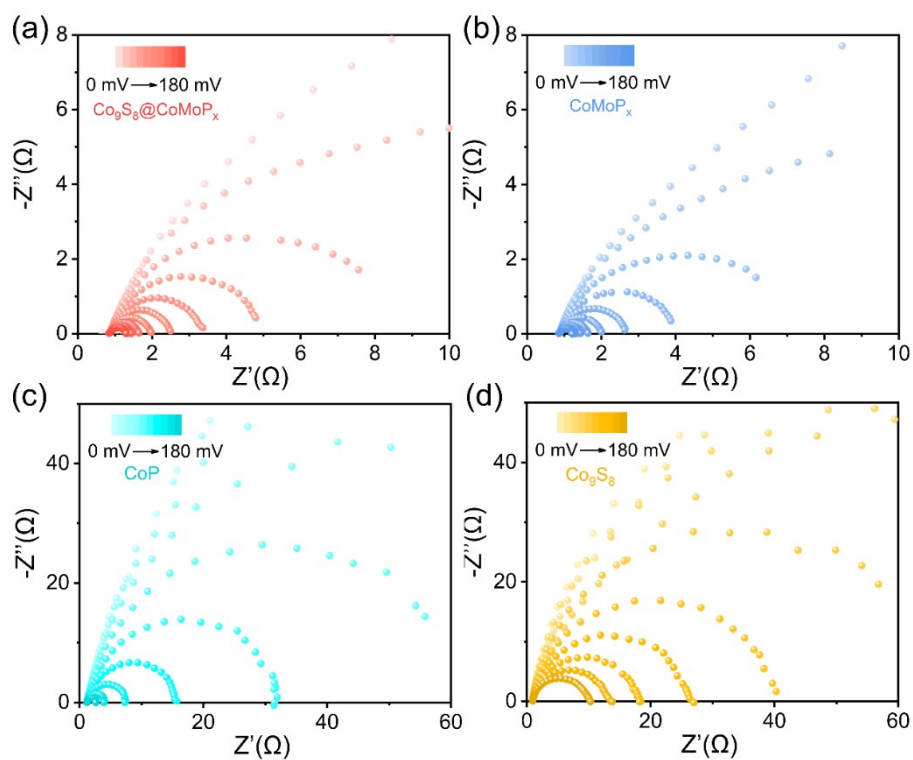**Fig. S12.** CV test of (a) $Co_9S_8@CoMoP_x$, (b) $CoMoP_x$, (c) CoP and (d) Co_9S_8 at 50 mV s^{-1} in 1.0 M KOH.

The peaks at low potentials can be attributed to the activation of Mo or electrochemical capacitance at large scan rate.

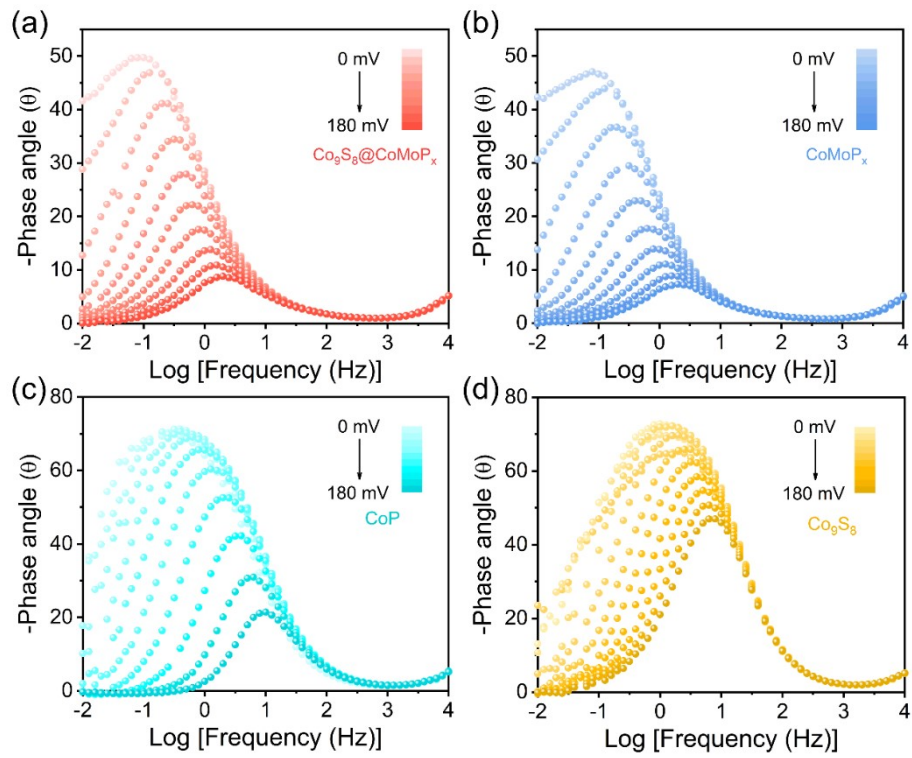**Fig. S13.** The LSV curves of different electrodes in 1.0 mol L^{-1} KOH with 95% iR-compensation.

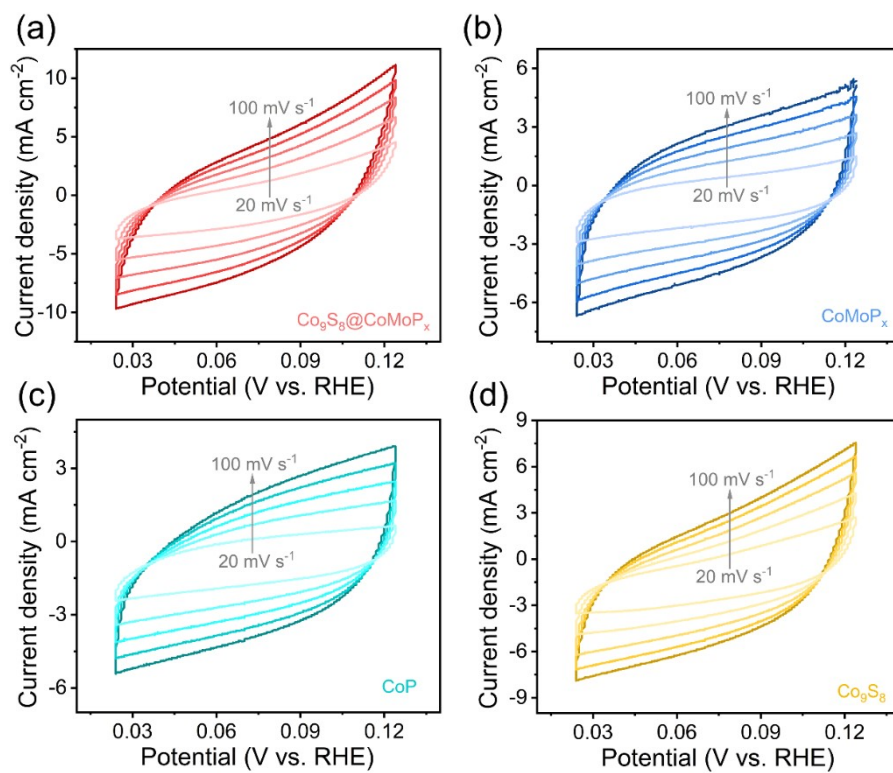**Fig. S14.** The EIS diagrams of (a) $Co_9S_8@CoMoP_x$, (b) $CoMoP_x$, (c) CoP and (d) Co_9S_8 at different overpotentials vs. RHE.

Fig. S15. The Bode phase plots of (a) $Co_9S_8@CoMoP_x$, (b) $CoMoP_x$, (c) CoP and (d) Co_9S_8 at different overpotentials vs. RHE.

Fig. S16. The CV curves of (a) $Co_9S_8@CoMoP_x$, (b) $CoMoP_x$, (c) CoP and (d) Co_9S_8 in the non-polarized region at different scan rates.
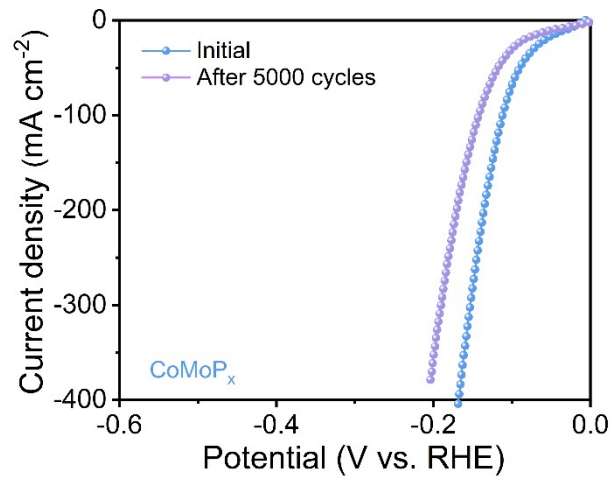
Fig. S17. The accelerated duration test of $CoMoP_x$ with 50 mV s^{-1} scan rate.
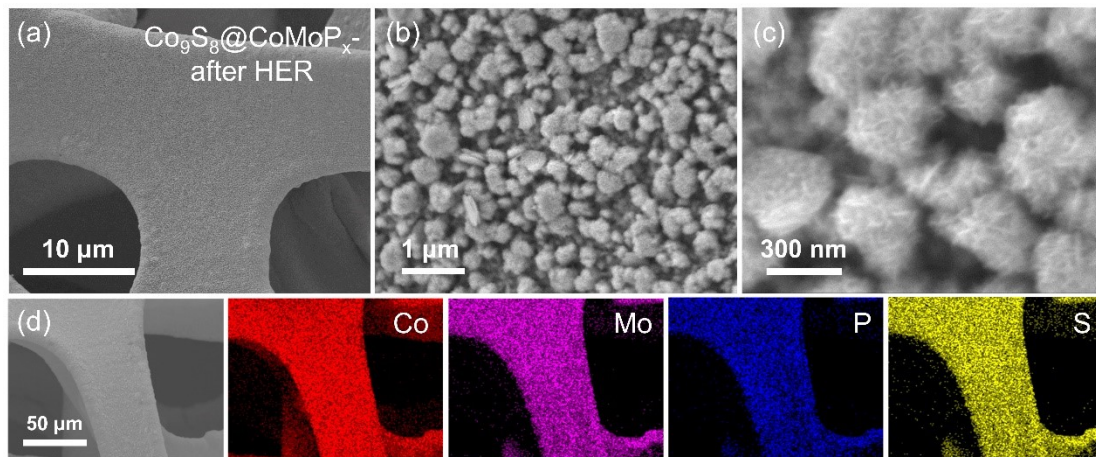
Fig. S18. (a-c) The SEM images of $Co_9S_8@CoMoP_x$ after chronopotentiometry test at different magnifications and (d) the corresponding EDS mappings of Co, Mo, P and S elements.
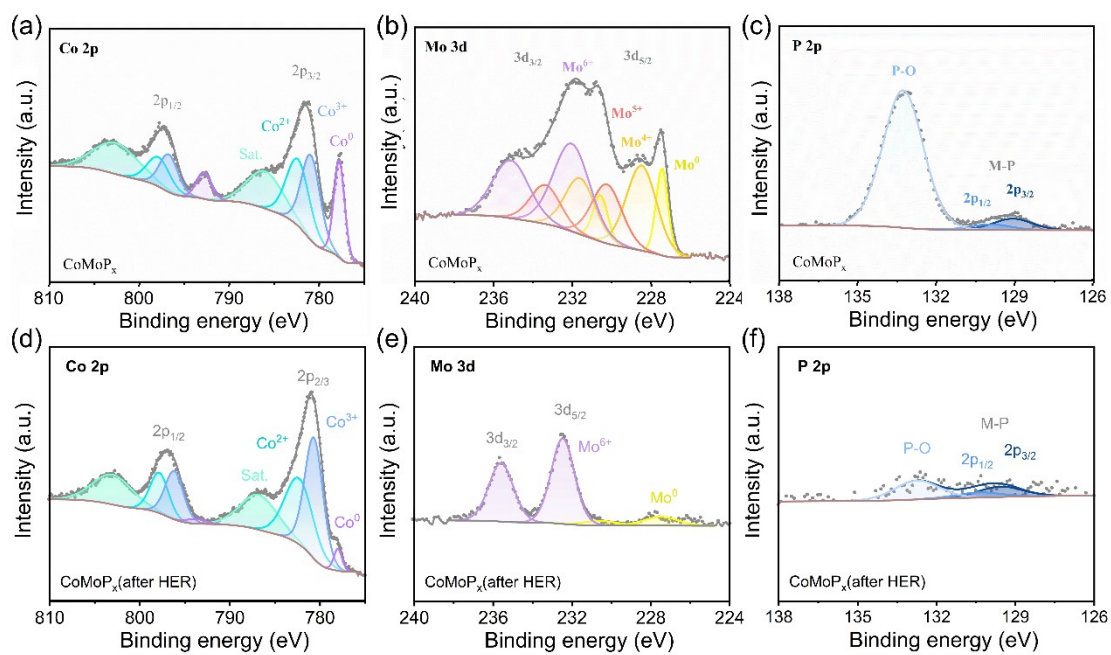
Fig. S19. The high resolution XPS spectra of (a) Co 2p, (b) P 2p for CoMoP$_x$ before HER progress, and (c) Co 2p, (d) P 2p for CoP after HER.
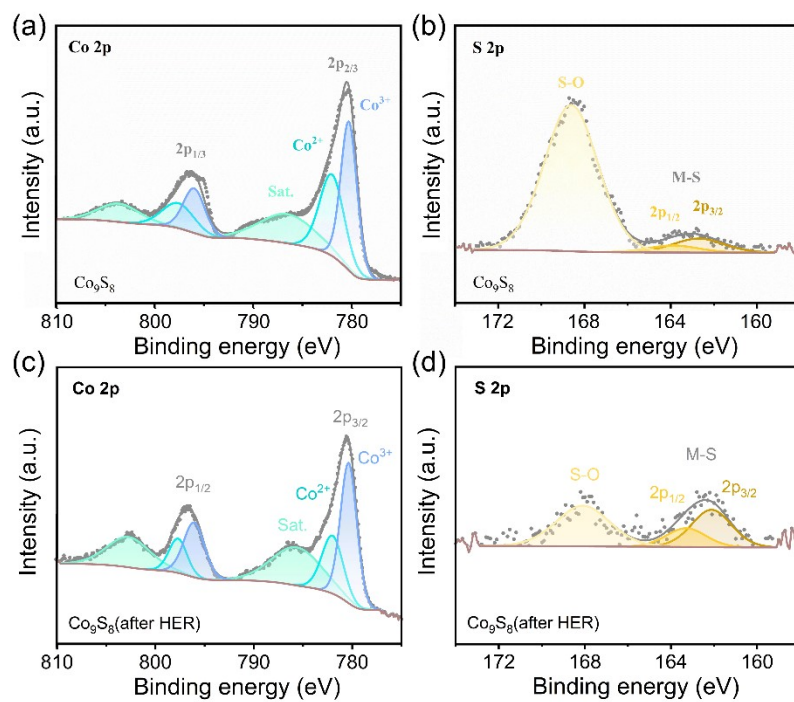
Fig. S20. The high resolution XPS spectra of (a) Co 2p, (b) P 2p for CoP before HER progress, and (c) Co 2p, (d) P 2p for Co_9S_8 after HER.
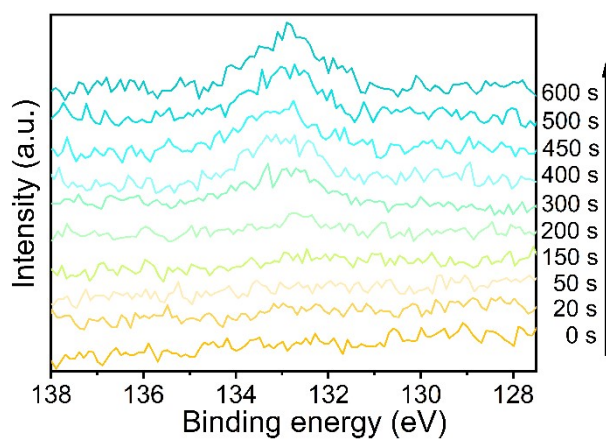
Fig. S21. XPS spectra of P 2p for $Co_9S_8@CoMoP_x$ after stability test at different etching levels.

As demonstrated in Fig. S24, the signal of P element appears as the etching time reach 300 s. The P 2p peak maintained with the increasing of etching times, manifesting existence of P element in bulk $Co_9S_8@CoMoP_x$ catalyst due to the protection role of Co_9S_8.

Fig. S22. The high resolution XPS spectra of (a) Co 2p, (b) P 2p for CoP before HER progress, and (c) Co 2p, (d) P 2p for CoP after HER.
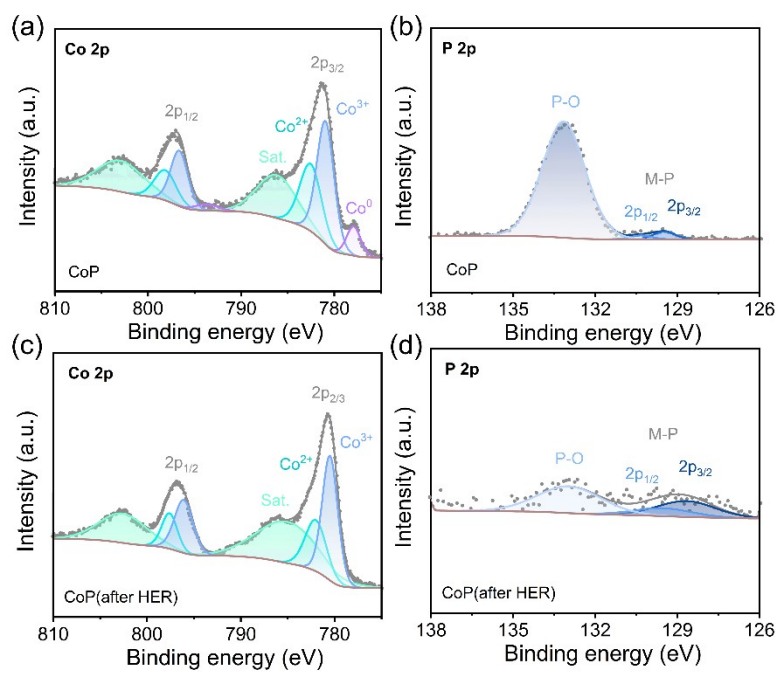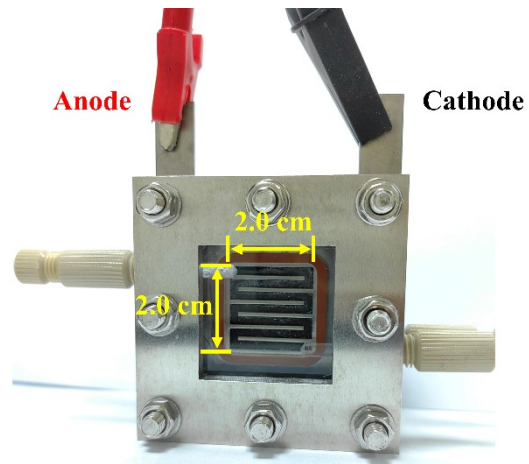
Fig. S23. The optical picture of AEMWE device.

Table S1. The ICP-OES results of Co, Mo, P and S in different electrocatalysts.

Electrode	Co content (mmol L^{-1})	Mo content (mmol L^{-1})	P content (mmol L^{-1})	S content (mmol L^{-1})
$CoMoP_x$	20.53	3.54	4.29	/
Co_9S_8	4.64	/	/	2.56
$Co_9S_8@CoMoP_x$	25.45	4.54	3.47	3.02

Table S2. The ICP-OES results of Co, Mo, P and S in different electrolytes.

Electrolyte	Co content (mmol L^{-1})	Mo content (mmol L^{-1})	P content (mmol L^{-1})	S content (mmol L^{-1})
Original 1 M KOH	0.0003	/	/	/
1 M KOH after Chronopotentiometry test of CoMoP$_x$	0.0033	0.0540	0.0638	/
1 M KOH after Chronopotentiometry test of Co$_9$S$_8$@CoMoP$_x$	0.0057	0.0195	0.0365	0.0238

Table S3. Comparison of HER performance of $Co_9S_8@CoMoP_x$ in this work and recently reported transition-metal-based catalysts.

Catalyst	Overpotential (mV)	Stability test current density (mA cm^{-2})	Stability duration (h)	Reference
$Co_9S_8@CoMoP_x$	**41@−10 mA cm^{-2}**	**−500**	**1000**	**This work**
	126@−100 mA cm^{-2}			
	226@−500 mA cm^{-2}			
CoMoP	62.3@−10 mA cm^{-2}	−200	55	Ref. [1]
MoS_2/Ni_2O_3H	84@−10 mA cm^{-2}	−10	45	Ref. [2]
	200@−217 mA cm^{-2}			
$CoP_3/CoMoP/NF$ HNAs	110@−10 mA cm^{-2}	−10	20	Ref. [3]
CoP/CoMoP	34@−10 mA cm^{-2}	−10	12	Ref. [4]
	94@−100 mA cm^{-2}			
CoS_2/MoS_2	76@−10 mA cm^{-2}	−400	16	Ref. [5]
Co_9S_8-MoS_2/NF	167@−10 mA cm^{-2}	−80	20	Ref. [6]
	250@−250 mA cm^{-2}			
$MoS_2/CoNi_2S_4$	78@−10 mA cm^{-2}	−10	48	Ref. [7]
	160@−100 mA cm^{-2}			
	190@−300 mA cm^{-2}			
5%La-CoMoP	49@−10 mA cm^{-2}	−10	20	Ref. [8]
CoMoP/CoP/NF	54@−10 mA cm^{-2}	−50	18	Ref. [9]
	127@−100 mA cm^{-2}			
NiFe-LDH@CoMo-P/NF	49@−10 mA cm^{-2}	−100	60	Ref. [10]
	138@−100 mA cm^{-2}			
Co-1T-MoS_2-bpe-350	118@−10 mA cm^{-2}	−20	50	Ref. [11]
	145@−100 mA cm^{-2}			

	239@−200 mA cm^{-2}			
CoMoP@C	81@−10 mA cm^{-2}	−10	24	Ref. [12]
NF@CoFeP	80@−10 mA cm^{-2}	−300	50	Ref. [13]
	145@−100 mA cm^{-2}			
Cu-FeOOH/Fe$_3$O$_4$	129@−100 mA cm^{-2}	−100	100	Ref. [14]
	285@−500 mA cm^{-2}			

3 Reference

1   H. Wang, C. Niu, W. Liu and S. Tao, *Appl. Catal., B*, 2024, **340**, 123249.

2   J. Hu, C. Zhang, Y. Zhang, B. Yang, Q. Qi, M. Sun, F. Zi, M. K. H. Leung and B. Huang, *Small*, 2020, **16**, 2002212.

3   D. Jiang, Y. Xu, R. Yang, D. Li, S. Meng and M. Chen, *ACS Sustainable Chem. Eng.*, 2019, **7**, 9309-9317.

4   X. Huang, X. Xu, X. Luan and D. Cheng, *Nano Energy*, 2020, **68**, 104332.

5   P. Liu, J. Yan, J. Mao, J. Li, D. Liang and W. Song, *J. Mater. Chem. A*, 2020, **8**, 11435-11441.

6   M. Kim, M. A. R. Anjum, M. Choi, H. Y. Jeong, S. H. Choi, N. Park and J. S. Lee, *Adv. Funct. Mater.*, 2020, **30**, 2002536.

7   J. Hu, C. Zhang, P. Yang, J. Xiao, T. Deng, Z. Liu, B. Huang, M. K. H. Leung and S. Yang, *Adv. Funct. Mater.*, 2019, **30**, 1908520.

8   L. Li, K. Chao, X. Liu and S. Zhou, *J. Alloy Compd.*, 2023, **941**, 168952.

9   Y. Wei, W. Li, D. Li, L. Yi and W. Hu, *Int. J. Hydrogen Energy*, 2022, **47**, 7783-7792.

10   D. Guo, H. Xia, X. Guo, L. Wen, T. Wang, X. Li and Z. Sun, *Int. J. Hydrogen Energy*, 2024, **79**, 73-85.

11   H. J. Liu, S. Zhang, Y. M. Chai and B. Dong, *Angew. Chem., Int. Ed.*, 2023, **62**, e202313845.

12   Y. Ma, C.-X. Wu, X.-J. Feng, H.-Q. Tan, L.-K. Yan, Y. Liu, Z.-H. Kang, E.-B. Wang and Y.-G. Li, *Energy Environ. Sci.*, 2017, **10**, 788-798.

13   J.-Z. Zhang, Z. Zhang, H.-B. Zhang, Y. Mei, F. Zhang, P.-X. Hou, C. Liu, H.-M. Cheng and J.-C. Li, *Nano Lett.*, 2023, **23**, 8331-8338.

14   C. Yang, W. Zhong, K. Shen, Q. Zhang, R. Zhao, H. Xiang, J. Wu, X. Li and N. Yang, *Adv. Energy Mater.*, 2022, **12**, 2200077.